Impact of gas composition on thermal conductivity of glass foams prepared via high-pressure sintering

Østergaard, Martin Bonderup; Petersen, Rasmus Rosenlund; König, Jakob; Bockowski, Michal; Yue, Yuanzheng

Published in:
Journal of Non-Crystalline Solids: X

DOI (link to publication from Publisher):
10.1016/j.nocx.2019.100014

Publication date:
2019

Document Version
Publisher's PDF, also known as Version of record

Journal of Non-Crystalline Solids: X 1 (2019) 100014

Contents lists available at ScienceDirect

Journal of Non-Crystalline Solids: X

journal homepage: www.journals.elsevier.com/journal-of-non-crystalline-solids-x

Impact of gas composition on thermal conductivity of glass foams prepared via high-pressure sintering

Martin B. Østergaard[a], Rasmus R. Petersen[a], Jakob König[b], Michal Bockowski[c], Yuanzheng Yue[a,*]

[a] Department of Chemistry and Bioscience, Aalborg University, DK-9220 Aalborg East, Denmark
[b] Advanced Materials Department, Jožef Stefan Institute, SI-1000 Ljubljana, Slovenia
[c] Institute of High-Pressure Physics, Polish Academy of Sciences, PL-01-142 Warsaw, Poland

ARTICLE INFO

Keywords:
Cathode ray tube panel glass
Glass foam
Gas composition
Thermal conductivity

ABSTRACT

Glass foam is a cellular material with excellent thermal insulating ability. The thermal conductivity (λ) of cellular materials is complex to understand because it is determined by the composition of the solid and gas phases, pore size, solid microstructure (amorphous or crystalline, struts, and walls), and radiation. In this paper, we focus on the influence of gas composition on λ of glass foams. Glass foams were prepared by a physical foaming approach, where powder pellets of cathode ray tube (CRT) panel glass were sintered at 640 °C in Ar or N_2 atmosphere at elevated pressure (5–25 MPa), and then cooled down to room temperature. When heating the sintered samples to the viscous state (approx. 10^8–10^6 Pa s corresponding to 650–740 °C), the high internal gas pressure in the closed pores expands the glass melt. We heat-treated each sintered sample multiple times in air at atmospheric pressure to gradually decrease the density, and thereby to obtain multiple λ values of each sample at different densities, while the chemistry of the sample remained almost identical. Gas chromatography revealed binary Ar-CO_2 and N_2-CO_2 gas compositions in the Ar- and N_2-sintered samples, respectively. The thermal conductivities of these gas mixtures ($\lambda_{gas,mix}$) were calculated to be 16.4 and 23.1 mW m^{-1} K^{-1}, presenting 22 and 31% of the effective λ for the Ar- and N_2-sintered samples, respectively. The lower $\lambda_{gas,mix}$ resulted in a lower λ of the Ar-sintered samples compared to the N_2-sintered ones at low density (< 0.6 g cm^{-3}). Therefore, it is crucial to control the gas composition for tailoring λ of low density glass foams.

1. Introduction

Glass foam is an attractive insulation material due to its low density, freeze-thaw-cycle resistance, non-flammability, chemical inertness, and superior mechanical strength compared to other insulation materials [1]. In most cases, glass foams are produced via a one-step thermochemical approach from a mixture of glass powder and foaming agent (s). Metal carbonates that decompose [2–4] and transition metal oxides, carbonaceous substances, and nitrides that reduce or oxidize [5–10] are often employed as foaming agents. At elevated temperatures, the foaming agents release gases into the viscous sintered glass body, causing expansion of the sample. Upon cooling the expanded melt freezes into a porous body [1]. For a successful foaming process a right match between glass melt viscosity (within the range $10^{3.3}$–10^6 Pa s) and the gas release temperature is required [11]. Another one-step method employs sol-gels for producing glass foams [12]. Two-step methods include dissolving and gelating of solid particles followed by heating at elevated temperatures [13], and a recently proposed physical approach enabling incorporation of inert gases [14,15]. For the physical foaming, the first step is to sinter glass powder under a high gas pressure, and the second step is to heat-treat the sintered body at elevated temperatures under ambient conditions causing expansion of the sample due to a high internal gas pressure.

The thermal conductivity (λ) is the most important property of glass foams when used for heat-insulation purposes. The heat transfer through porous materials can be viewed as a sum of individual contributions from the conduction of solid matrix, conduction of gas phase, thermal radiation, and convection [16]. The radiation and convection can be neglected due to high density of the glass phase (relative contribution of < 15% for densities > 40 kg m^{-3}) [17,18] and the small pores (diameter < 4 mm) [19], respectively. The solid phase is primarily amorphous, though, crystalline phases can be present, originating either from the foaming agents or from crystallization of the glass during the foaming process [20–22]. Crystals have a higher λ than their amorphous counterparts [23], and even a small amount of crystals in an amorphous matrix increases the λ [24]. Therefore, presence of

* Corresponding author.
E-mail address: yy@bio.aau.dk (Y. Yue).

https://doi.org/10.1016/j.nocx.2019.100014
Received 21 December 2018; Received in revised form 11 February 2019; Accepted 13 February 2019
Available online 27 February 2019

crystals is undesired. Additionally, the type of glass cullet used for preparing glass foams have a significant impact on the λ of low density glass foams [6]. The gas phase can be changed by use of different foaming agents resulting in, e.g., O_2, CO, or CO_2 in the gas phase. However, only few studies dealed with analysis of the actual gas composition of glass foams. Recently, the gases generated during foaming of CRT panel glass–Mn_xO_y–C systems with different carbon sources were determined to be mainly CO_2 for carbon black and CO for activated carbon, where the CO content increases with increasing temperature [25]. In post-foaming analyses, glass foams prepared from glass mixtures (CRT panel, flat, window, and container glasses) using Fe_2O_3 and carbon black as foaming agents involved mainly CO_2 in the closed pores of CRT panel glass containing samples (> 90 vol%), while samples without CRT panel glass contained < 77 vol% CO_2 in the closed pores [6]. Other parameters that influence the insulation properties of glass foams, like average pore size, have also been investigated [26–28]. So far there has been no attempt to examine the influence of the gas composition on the λ. In order to do so, the foam characteristics such as foam density/porosity and solid composition should be kept unchanged since they affect the λ of porous materials [21,29,30].

In this study we prepared glass foams by a physical foaming approach [14,15] in order to control the chemical compositions of the solid and the gas phase in the glass foam. CRT panel glass pellets were sintered under a high Ar or N_2 pressure (5–25 MPa) and reheated at ambient conditions, generating glass foams with mainly Ar or N_2 in the gas phase. Ar and N_2 have thermal conductivities similar to those of CO_2 and O_2, respectively, which can be obtained by a thermo-chemical approach. We demonstrate the impact of the gas composition on the λ of glass foams.

2. Experimental

2.1. Sample preparation

CRT panel glass powder with a composition (in wt%) 61.04SiO_2-2.37Al_2O_3-7.74Na_2O-7.11K_2O-0.84CaO-0.32MgO-1.52ZrO_2-9.66BaO-7.82SrO and trace amounts of TiO_2, Fe_2O_3, ZnO, PbO, and Sb_2O_3 [21] was used to produce glass foams. 20 g of glass powder (particle size D_{90} = 26.73 μm) was uniaxially pressed into green bodies with diameter of 35 mm. The green bodies were sintered in a graphite crucible in a multizone cylindrical furnace under a controlled gas pressure using Ar or N_2 (purity 5.0) [31]. The samples were heated to 640 °C at 10 °C min^{-1} and heat-treated for 30 min. The sintering was carried out under isostatic pressures of 5, 10, 15, 20, or 25 MPa. After sintering, the chamber was cooled at 60 °C min^{-1} to room temperature, and then decompressed at 30 MPa min^{-1} to atmospheric pressure.

The samples subjected to high pressure sintering were reheated at ambient conditions in an electrical tube furnace at 10 °C min^{-1} to 650 °C, heat-treated for 15 min, and then cooled below 500 °C at 10 °C min^{-1}. The samples were characterized with respect to density, thermal conductivity, gas composition, and crystallization as described in the next section. After characterization, the glass foams were again reheated to higher temperatures (i.e., 665, 680, 695, 710, 725, and 740 °C), heat-treated for 15 min, followed by cooling to room temperature. The samples were characterized after each heat-treatment for density and thermal conductivity.

The top surface of the samples was grinded and plane polished after the first heat-treatment in order to ensure a plane contact between the sample and the sensor during thermal conductivity measurements. The surface of the sample was plane polished after each heat treatment to ensure a plane surface prior to thermal conductivity measurement. Only samples sintered at 5–20 MPa were used for analyses after the first heat-treatment, as the high internal pressure caused breakage of the samples sintered at 25 MPa. For the Ar-sintered sample the breakage occurred during the sintering treatment while the N_2-sintered sample broke during the first heat-treatment process.

2.2. Foam characterization

The foam density (ρ_{foam}) was determined using Archimedes' principle with water as immersion medium. The skeletal density (ρ_{skel}) was determined similarly, but with ethanol as immersion medium. Porosity (ϕ) and closed porosity (ϕ_{CP}) were calculated using Eqs. (1) and (2), respectively. The powder density (ρ_{pow}) of the CRT panel glass was determined to be 2.76 g cm^{-3} using a He-pycnometer (Ultrapyc 1200e, Quantachrome).

$$\phi = \left(1 - \frac{\rho_{foam}}{\rho_{pow}}\right) \cdot 100\% \quad (1)$$

$$\phi_{CP} = \frac{\rho_{skel}^{-1} - \rho_{pow}^{-1}}{\rho_{foam}^{-1} - \rho_{pow}^{-1}} \cdot 100\% \quad (2)$$

The pore structure was analyzed on gold-coated glass foam pieces after the first (650 °C) and last (740 °C) heat-treatment using a scanning electron microscope (SEM) (1540 XB, Zeiss) operating at 10 kV.

A method based on the transient plane source technique (TPS 2500 S, Hot Disk AB) was established to measure the thermal conductivity (λ) of the glass foams. The Hot Disk method allows to measure in isotropic mode, where a flat sensor is placed between two identical samples. In a single-sided mode, the flat sensor is placed between a sample and an insulating reference sample with known thermal conductivity and thermal diffusivity. To be able to measure λ of the glass foams, we extended the capability range of the single-sided mode by doing the following. The λ of commercial glass foam products (produced by Pittsburg Corning Corporation, USA) and calcium silicate products (produced by Skamol, Denmark) was measured in both the isotropic mode and in the single-sided mode using a polystyrene sample (National Institute of Standards and Technology, USA) as the reference insulating material. A linear relationship ($\lambda_{ss} = 0.9978 \cdot \lambda_{iso} + 4.3$) was established between the λ_{ss} values measured by the single-sided mode and λ_{iso} by the isotropic mode (Fig. 1). The intercept (4.3 mW m^{-1} K^{-1}) was subtracted the λ_{ss} values in order to correct the λ_{ss} data of the glass foam samples. All the measurements were performed with a Kapton sensor 8563 (radius of 9.868 mm) at 25.4 ± 0.1 °C. The temperature was controlled by using a climate chamber (WKL 100, Weiss, Germany). Each sample was measured five times with 15 min intervals to ensure temperature equilibration for the sample between each measurement. Furthermore, the measurement time and power output were adjusted for each sample to prevent overheating and to maintain the total time within the correct time window [32]. The Kapton™ insulation

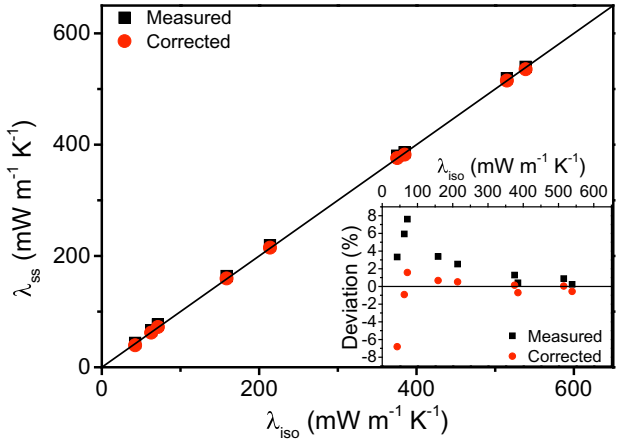

Fig. 1. Comparison between the λ_{iso} values measured by the isotropic mode and the corrected λ_{ss} values measured by the single-sided mode. The correction was done by subtraction of the intercept (4.3 mW m^{-1} K^{-1}) from the measured data points. The line represents a standard line ($\lambda_{iso} = \lambda_{ss}$). Inset: Deviation of the measured λ_{ss} values from the corrected ones. The standard deviation of the measured data points is smaller than the size of the symbols.

of the sensor causes a contact resistance between the sensor and the samples during measurements. The contact resistance has a constant influence on the temperature increase after a short time [33] and therefore the initial data points were removed.

Gas composition and pressure in the closed pores after heating to the final maximum temperature were assessed by crushing approximately one quarter of a sample in an evacuated, He-filled cylinder connected to a pressure gauge, and subsequent gas analysis using gas chromatography. A gas volume of 0.3 mL was ejected from the crushing cell and injected into a gas chromatograph (7890A GC System, Agilent Technologies). The gas chromatograph has a split column consisting of a Rt-Msieve™ 5A column (Restek) with a length of 30 m and an inner diameter of 0.320 mm and a Rt-QPLOT™ (Restek) with a length of 30 m and an inner diameter of 0.530 mm. The gases were detected with a thermal conductivity detector (TCD). The oven and inlet temperatures were 80 and 200 °C, respectively. The carrier gas was helium (purity 6.0). ChemStation software (Agilent Technology) was used for data acquisition and peak integration. The detection limit was 1 μV s (integrated peak). First, background signals from the crushing cell were measured, followed by crushing of the glass foam, and then the gas from the crushing cell containing released gases was analyzed. The N_2, O_2, and CO_2 contents were calculated based on standard curves, and the Ar content was calculated as the remaining gas ($V_{Ar} = V_{gas}$-V_{N2}-V_{O2}-V_{CO2}). As Ar and O_2 peaks overlap, the O_2 content in the Ar samples was calculated based on the N_2:O_2-ratio in the atmosphere (i.e., 3.73:1). The detected atmospheric air (N_2 and O_2) originated from minor contamination of the cell (most probably occurring during crushing of the samples), therefore, it was subtracted from the final gas composition. The final composition was given as a binary gas mixture containing the sintering gas (Ar or N_2) and CO_2. The composition was calculated as Ar/(Ar + CO_2) and CO_2/(Ar + CO_2) for the Ar-sintered samples and N_2/(N_2 + CO_2) and CO_2/(N_2 + CO_2) for the N_2-sintered samples.

The pressure in the closed pores was calculated through Boyle's law from the volume released by crushing, the free volume of the cell, and the change in pressure before and after crushing. The uncertainty of the measurement was ± 2%.

Crystalline phases in the glass foams were analyzed after the first and the final heat-treatment by powder X-ray diffraction (XRD) using an Empyrean diffractometer (PANalytical). Data were obtained in the 2θ range of 10°–70° with a step size of 0.013°.

3. Results and discussion

Heat-treatment of the sintered samples causes an expansion of the samples due to the high internal gas pressure [15]. The foam density of the samples reheated after sintering at 650 °C is shown in Fig. 2. It can be seen that an increasing pressure results in a lower density up to 15 and 20 MPa for Ar and N_2, respectively, followed by a small increase. This is in good agreement with previous findings on smaller samples [14,15]. The Ar- and N_2-sintered samples exhibit similar densities for pressures ranging from 10 to 25 MPa, whereas for a pressure of 5 MPa the Ar-sintered sample has a higher density compared to the N_2-sintered sample. The porosity has an inverse relation to the foam density, with maximum porosity of 84–87% for samples sintered at 15–25 MPa for both Ar and N_2 (Table 1). The samples have closed porosity of 100% after the first reheating at 650 °C (Table 1).

Table 1
Foam density (ρ_{foam}), porosity (ϕ), and closed porosity (ϕ_{CP}) of the samples heat treated in air at 650 °C. Prior to the heat-treatment the samples were sintered in either Ar or N_2 at pressures of 5–25 MPa. The error ranges of ρ_{foam}, ϕ, and ϕ_{CP} are ± 0.03 g cm^{-3}, ± 1% point, and ± 1% point, respectively.

Gas type	Pressure (MPa)	ρ_{foam} (g cm^{-3})	ϕ (%)	ϕ_{CP} (%)
Ar	5	0.99	64	99
	10	0.59	79	99
	15	0.37	87	100
	20	0.41	85	100
	25	0.42	84	100
N_2	5	0.84	70	100
	10	0.60	78	100
	15	0.44	84	100
	20	0.41	85	100
	25	0.45	84	100

The foam density decreases when the samples are exposed to higher maximum temperatures (T_{MAX}) (Fig. 3). A higher T_{MAX} results in a

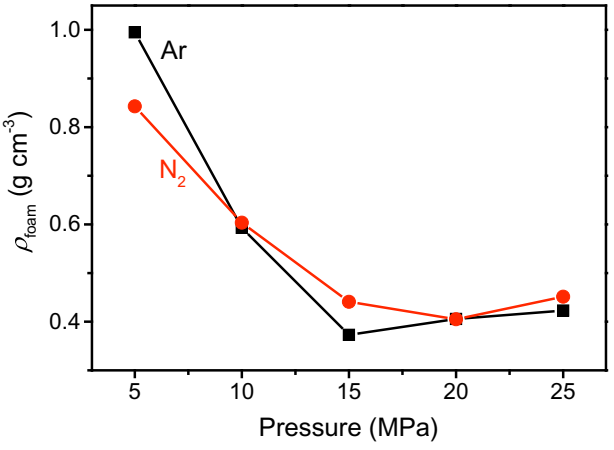

Fig. 2. Foam density (ρ_{foam}) of samples sintered in Ar or N_2 at gas pressures of 5–25 MPa, followed by expansion in air at 650 °C. The error of ρ_{foam} is ± 0.03 g cm^{-3}.

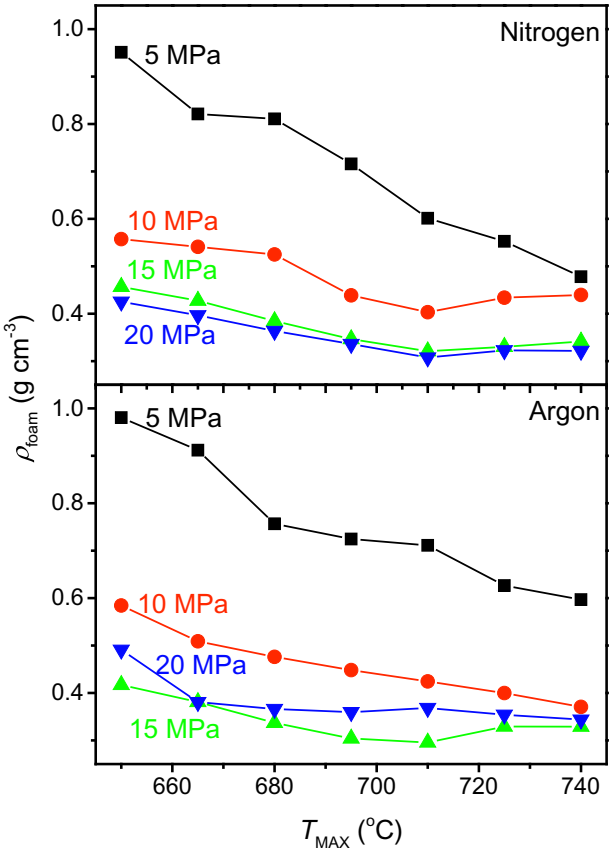

Fig. 3. Change in the foam density (ρ_{foam}) of the samples heated multiple times to different maximum temperatures (T_{MAX}) in air after sintering in Ar or N_2. The error of ρ_{foam} is ± 0.03 g cm^{-3}, and it is smaller than the size of the symbols.

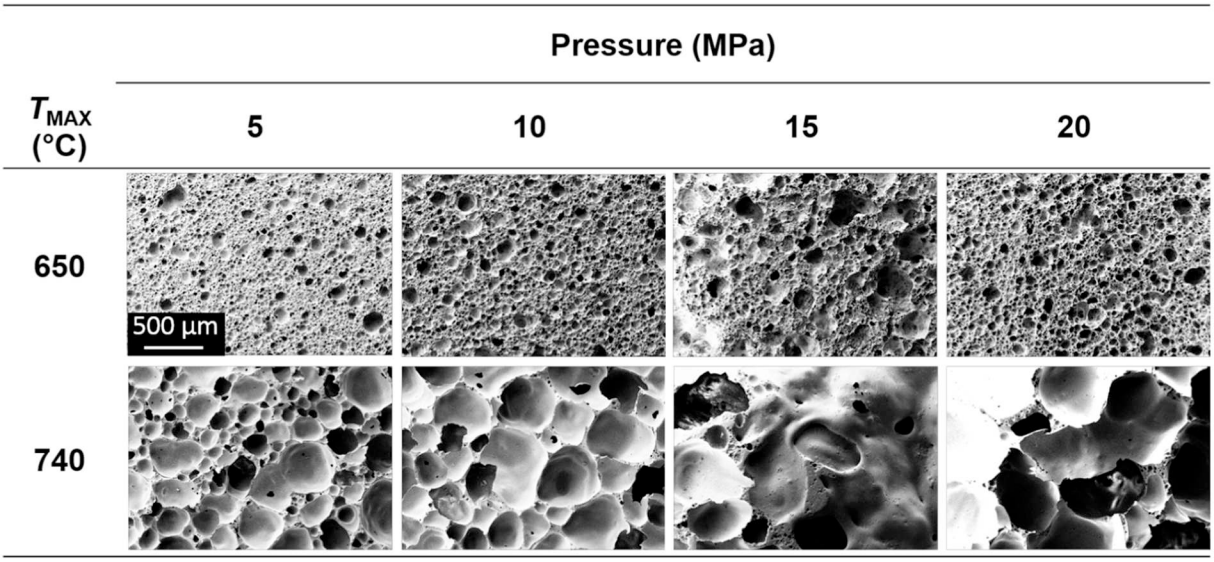

Fig. 4. Pore structure of the glass foams heated to T_{MAX} of 650 °C and after heating the samples seven times with a 15 °C increments from 650 to 740 °C for samples sintered under Ar pressure of 5–20 MPa. A scale bar is shown in the upper-left image.

lower viscosity of the glass, allowing a greater expansion of the glass melt with the high internal gas pressure. However, a minimum in foam density is found at 710 °C for the 10–20 MPa N_2-sintered samples. A similar minimum is found for the 15 MPa Ar-sintered sample, whereas the density of the 10 MPa sintered sample continuously decreases and the 20 MPa sintered sample reaches a constant density above 665 °C. The minima in density for the samples sintered at high gas pressures (10–20 MPa) are most probably caused by collapse or breakage of pore walls due to the lower viscosity at higher temperatures. In the samples sintered at 5 MPa, the pressure in the pores is so small that it gives only weak force to expand the pore.

The pore size increases with increasing the sintering pressure, reaching a maximum at 15 MPa for Ar-sintered samples (Fig. 4) and 20 MPa for N_2-sintered samples. This is observed both for samples heated at 650 °C, and for samples reaching a final T_{MAX} of 740 °C after seven heat treatments. Comparison of the pore sizes of the same sample heated to different temperatures shows that the size of the pores increases with increasing T_{MAX}. The pores expand due to the decreasing viscosity at higher temperatures, allowing the internal gas pressure to expand the glass phase more easily. The coalescence of pores increases the pore size. This process is very dependent on viscosity and progresses faster at elevated temperatures in the foaming process of glass melts.

The thermal conductivity (λ) of the glass foams decreases with the foam density (Fig. 5). The effect of sintering pressure is initially reflected in the different foam density of the samples reheated to specific T_{MAX} as a higher pressure results in lower density, while this trend diminishes at higher reheating temperatures (Fig. 3). For all the samples, a minimum in the λ is obtained at a sintering pressure of 15 MPa. In general, λ of gases increases with pressure [34–36], however, with increasing T_{MAX}, the pressure in the pores drops and is very similar in all samples after final heat-treatment (Table 2). Thus λ is not a function of the sintering pressure, but solely a function of the density under the assumption that the pore size is similar for different samples, thus the sintering pressure has no influence on λ. It is also possible that the gas composition varies with an increase in T_{MAX}. In this study, the cell gas pressure and composition were measured only after the final heat-treatment, thus the final confirmation of the gas composition effect is missing.

The gas phase of all glass foams consists of the compression gas (Ar or N_2) and CO_2. The presence of CO_2 could be attributed to two possible contaminations. First, residues of the organic coating on the panel glass, and second, carbon contamination from the graphite crucible during

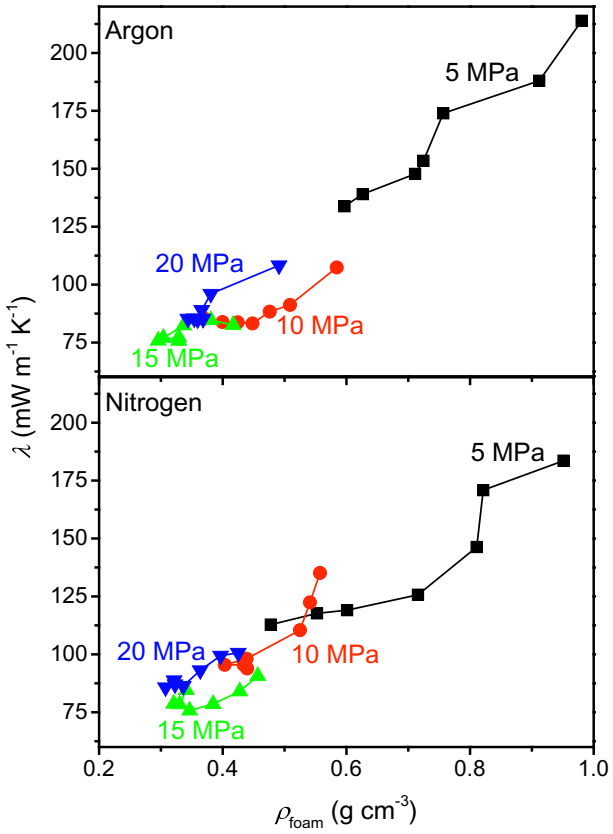

Fig. 5. Thermal conductivity (λ) of glass foams with different densities (ρ_{foam}). The glass foams are prepared by high pressure sintering in Ar or N_2 using gas pressures of 5, 10, 15, or 20 MPa. The samples are reheated seven times in the range 650–740 °C with 15 °C increments. The errors of λ and ρ_{foam} are smaller than the symbols.

the sintering process. During foaming, the carbon reacted with oxygen from the glass (e.g., from oxidation processes involving Fe and Sb). The cross-section of a sintered sample shows that the sample is slightly colored and bears a surface layer (2–3 mm in thickness), suggesting the presence of carbon and a decreasing carbon concentration towards the

Table 2
Normalized gas composition ($V_{Ar} + V_{CO2} = 1$ and $V_{N2} + V_{CO2} = 1$) (vol%) of glass foams heat-treated seven times to different temperatures (in the range between 650 and 740 °C). The thermal conductivity of the binary gas mixtures ($\lambda_{gas,mix}$) are calculated through Eqs. (3) and (4) for 25.4 °C. The cell pressure (P_{cell}) is calculated from Boyle's law. Errors on the individual gas species are below ± 2 vol% and on P_{cell} are ± 2%.

Gas type	Pressure (MPa)	Ar (vol%)	CO_2 (vol%)	N_2 (vol%)	$\lambda_{gas,mix}$ (mW m^{-1} K^{-1})	P_{cell} (bar)
Ar	5	69.9	30.1	–	16.4	0.20
	10	70.5	29.5	–	16.4	0.18
	15	76.5	23.5	–	16.4	0.20
	20	71.6	28.4	–	16.4	0.19
N_2	5	–	16.1	83.9	23.1	0.19
	10	–	17.0	83.0	23.1	0.18
	15	–	12.2	87.8	23.1	0.19
	20	–	13.4	86.6	23.1	0.17

center of the sample. Due to the pronounced presence of CO_2 in the cells, λ of gaseous phase was calculated using an empirical model proposed by Wassiljewa [37]. Therefore, the binary gas compositions are calculated based on the Ar/CO_2 content and N_2/CO_2 content for Ar-sintered and N_2-sintered samples, respectively (Table 2). The thermal conductivities of Ar, N_2, and CO_2 at 25 °C are 17.6 mW m^{-1} K^{-1} [38], 26.4 mW m^{-1} K^{-1} [39], and 16.3 mW m^{-1} K^{-1} [40], respectively. The thermal conductivity of binary gas mixtures ($\lambda_{gas,mix}$) is calculated as follows:

$$\lambda_{gas,mix} = \sum_{i=1}^{n} \frac{x_i \lambda_i}{\sum_{j=1}^{n} x_j \theta_{ij}} \quad (3)$$

where x is the mole fraction of each gas, λ_i is the thermal conductivity of gas specie i, and θ_{ij} is the binary interaction parameter between gas i and gas j found from following equation (Eq. (4)) [41]:

$$\theta_{ij} = \frac{\varepsilon\left[1 + \left(\frac{\lambda_i}{\lambda_j}\right)^{0.5}\left(\frac{MW_j}{MW_i}\right)^{0.25}\right]^2}{\left[8\left(1 + \frac{MW_i}{MW_j}\right)\right]^{0.5}} \quad (4)$$

where MW is the molecular weight of each gas specie, and ε is a numerical constant approx. 1 [42].

The gas composition in the samples sintered in Ar or N_2 gases under different pressures is very similar thus the difference in the calculated gaseous thermal conductivity is negligible (Table 2). The calculated

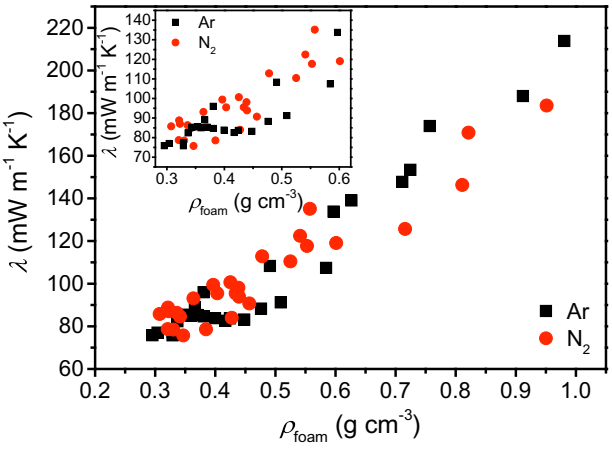

Fig. 6. Thermal conductivity (λ) of glass foams prepared by high pressure sintering in Ar and N_2 and reheating in the range between 650 and 740 °C at atmospheric conditions. Inset zooms in on the low-density area (< 0.6 g cm^{-3}). The error of λ and ρ_{foam} is smaller than the symbols.

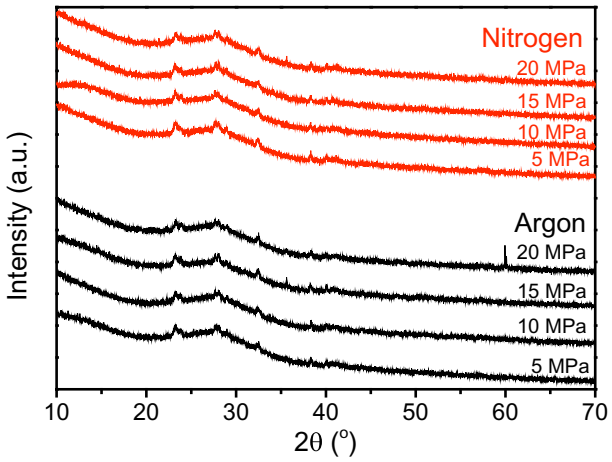

Fig. 7. XRD patterns of crushed glass foams after seven heat-treatments between 650 °C and 740 °C for 15 min. The diffraction patterns are shifted vertically for clarity.

$\lambda_{gas,mix}$ is 16.4 mW m^{-1} K^{-1} and 23.1 mW m^{-1} K^{-1} for Ar-sintered and N_2-sintered samples, respectively. Similar gas compositions were previously analyzed and calculated by Yorizane et al. [43] reporting a value of 16.9 mW m^{-1} K^{-1} for binary Ar-CO_2 gas mixture with CO_2 content of 28.6% and 30.1% at 1 bar and 25.4 °C. Hence, the calculated values are in reasonable agreement with literature values. In general, the $\lambda_{gas,mix}$ of the gas phase shows to be significant lower for Ar-sintered samples than N_2-sintered samples which can used to explain difference in thermal conductivity of glass foams.

In general, λ is lower for Ar-sintered samples compared to N_2-sintered ones for densities < 0.6 g cm^{-3}, while it is opposite for densities > 0.6 g cm^{-3} (Fig. 6). For the low-density samples (< 0.6 g cm^{-3}), the results are in accordance with the lower λ of Ar-sintered samples compared to λ of N_2-sintered samples. For high-density samples (> 0.6 g cm^{-3}), other factors must play a role, e.g., the pore size (Fig. 3) as suggested elsewhere [26,27]. The gaseous contribution to the effective thermal conductivity is higher at lower densities. For the samples with the lowest density, the relative gaseous contributions ($\lambda_{gas,mix}/\lambda$) are 22% and 31% for Ar and N_2, respectively. The pressure of the gas in the cells (P_{cell}) does not influence the thermal conductivity of the glass foams at higher reheating temperatures (i.e., low densities) as all values are in the range of 0.17 to 0.20 bar (Table 2). However, it is likely that P_{cell} is higher for samples reheated at lower temperatures, leading to a higher gas contribution to the λ of high density foams.

All the glass foams were found to be glassy after the initial heat treatment at 650 °C as previously shown for one-time reheated samples prepared under same pressures [15]. However, the XRD results (Fig. 7) indicate presence of a small amount of crystals in the samples after multiple heat-treatments between 650 and 740 °C. The crystal content is very similar in all the samples. However, the diffraction peaks are too small to identify the crystalline phases. Bulk oxide glasses treated under high pressure (1 GPa) at 1.15T_g for 30 min or 0.9T_g for up to 10,000 min show no pressure induced crystallization [44], suggesting that the crystallization observed in this study is thermally induced.

XRD analyses were performed after the first and the last heat-treatment, thus it is unknown when the crystallization occurs. However, the presence of the crystals could be part of the reasons for the increase in λ with decreasing foam density, e.g., the 15 MPa N_2-sintered sample at densities < 0.35 g cm^{-3} (Fig. 5), as higher crystallinity increases λ [24].

4. Conclusion

Glass foams were prepared by heat-treating CRT panel glass pellets

sintered under high gas pressure (5–25 MPa) using Ar or N_2, under atmospheric conditions. A minimum in foam density was found for the samples sintered at a gas pressure of 15–20 MPa. The obtained glass foams exhibit a closed pore structure. In general, the thermal conductivity (λ) of the glass foams decreases with decreasing foam density, with few exceptions for low densities $< 0.40\ g\ cm^{-3}$. The increase in λ at low density is probably caused by the crystallization or change in pore size. The gas in the glass foam after final reheating consists of the gas used during the sintering (Ar or N_2) and CO_2. The thermal conductivity of the gas mixtures ($\lambda_{gas,mix}$) are calculated to be $16.4\ mW\ m^{-1}\ K^{-1}$ and $23.1\ mW\ m^{-1}\ K^{-1}$ for Ar-sintered and N_2-sintered samples, respectively. This difference implies an influence of the gas phase, Ar versus N_2, on the λ of glass foams. For densities $< 0.6\ g\ cm^{-3}$ the Ar-sintered samples show lower λ than the N_2-sintered ones, demonstrating that incorporating low thermal conductive gases into glass foams is an important way to minimize the effective λ of low density glass foams. To better understand the mechanism of heat transfer through glass foams, glass foams with different gas phases (ideally pure gases), a lower density ($< 0.15\ g\ cm^{-3}$), and similar pore structure should be studied in the future.

Acknowledgement

M.B.Ø., R.R.P., J.K., and Y.-Z.Y. thank the Energy Technology Development and Demonstration Programme (EUDP) for financial support (64015-0018). We thank Sonja Haastrup Merrild (Skamol A/S) for providing calcium silicate samples.

Declaration of interests

The authors declare that they have no known competing financial interests or personal relationships that could have appeared to influence the work reported in this paper.

References

[1] G. Scarinci, G. Brusatin, E. Bernardo, Glass foams, in: M. Scheffler, P. Colombo (Eds.), Cell. Ceram. Struct. Manuf. Prop. Appl, Wiley-VCH Verlag GmbH & Co KGaA, Weinheim, 2005, pp. 158–176.
[2] R.R. Petersen, J. König, M.M. Smedskjaer, Y. Yue, Effect of Na_2CO_3 as foaming agent on dynamics and structure of foam glass melts, J. Non-Cryst. Solids 400 (2014) 1–5.
[3] J. König, R.R. Petersen, Y. Yue, Influence of the glass–calcium carbonate mixture's characteristics on the foaming process and the properties of the foam glass, J. Eur. Ceram. Soc. 34 (2014) 1591–1598.
[4] V. Ducman, M. Kovacevic, The foaming of waste glass, Key Eng. Mater. 132–136 (1997) 2264–2267.
[5] M.B. Østergaard, R.R. Petersen, J. König, Y. Yue, Effect of alkali phosphate content on foaming of CRT panel glass using Mn_3O_4 and carbon as foaming agents, J. Non-Cryst. Solids 482 (2018) 217–222.
[6] J. König, R.R. Petersen, N. Iversen, Y. Yue, Suppressing the effect of cullet composition on the formation and properties of foamed glass, Ceram. Int. 44 (2018) 11143–11150.
[7] V. Laur, R. Benzerga, R. Lebullenger, L. Le Gendre, G. Lanoë, A. Sharaiha, P. Queffelec, Green foams for microwave absorbing applications: synthesis and characterization, Mater. Res. Bull. 96 (2017) 100–106.
[8] M.S. Heydari, S.M. Mirkazemi, S. Abbasi, Influence of Co_3O_4, Fe_2O_3 and SiC on microstructure and properties of glass foam from waste cathode ray tube display panel (CRT), Adv. Appl. Ceram. 113 (2014) 234–239.
[9] A.S. Llaudis, M.J.O. Tari, F.J.G. Ten, E. Bernardo, P. Colombo, Foaming of flat glass cullet using Si_3N_4 and MnO_2 powders, Ceram. Int. 35 (2009) 1953–1959.
[10] J.P. Wu, A.R. Boccaccini, P.D. Lee, M.J. Kershaw, R.D. Rawlings, Glass ceramic foams from coal ash and waste glass: production and characterisation, Adv. Appl. Ceram. 105 (2006) 32–39.
[11] R.R. Petersen, J. König, Y. Yue, The viscosity window of the silicate glass foam production, J. Non-Cryst. Solids 456 (2017) 49–54.
[12] R. Gupta, A. Kumar, Bioactive materials for biomedical applications using sol-gel technology, Biomed. Mater. 3 (2008) 034005.
[13] A. Rincón, G. Giacomello, M. Pasetto, E. Bernardo, Novel 'inorganic gel casting' process for the manufacturing of glass foams, J. Eur. Ceram. Soc. 37 (2017) 2227–2234.
[14] B. Wang, K. Matsumaru, J. Yang, Z. Fu, K. Ishizaki, Mechanical behavior of cellular borosilicate glass with pressurized Ar-filled closed pores, Acta Mater. 60 (2012) 4185–4193.
[15] M.B. Østergaard, R.R. Petersen, J. König, M. Bockowski, Y. Yue, Foam glass obtained through high-pressure sintering, J. Am. Ceram. Soc. 101 (2018) 3917–3923.
[16] D.K. Hale, The physical properties of composite materials, J. Mater. Sci. 11 (1976) 2105–2141.
[17] B.K. Larkin, S.W. Churchill, Heat transfer by radiation through porous insulations, AICHE J. 5 (1959) 467–474.
[18] E. Placido, M.C. Arduini-Schuster, J. Kuhn, Thermal properties predictive model for insulating foams, Infrared Phys. Technol. 46 (2005) 219–231.
[19] R.E. Skochdopole, The thermal conductivity of foamed plastics, Chem. Eng. Prog. 57 (1961) 55–59.
[20] R.R. Petersen, J. König, M.M. Smedskjaer, Y. Yue, Foaming of CRT panel glass powder using Na_2CO_3, Glas. Technol. Eur. J. Glas. Sci. Technol. A. 55 (2014) 1–6.
[21] R.R. Petersen, J. König, Y. Yue, The mechanism of foaming and thermal conductivity of glasses foamed with MnO_2, J. Non-Cryst. Solids 425 (2015) 74–82.
[22] E. Bernardo, G. Scarinci, S. Hreglich, Foam glass as a way of recycling glasses from cathode ray tubes, Glas. Sci. Technol. 78 (2005) 7–11.
[23] C. Kittel, Interpretation of the thermal conductivity of glasses, Phys. Rev. 755 (1949) 972–974.
[24] M.B. Østergaard, R.R. Petersen, J. König, H. Johra, Y. Yue, Influence of foaming agents on thermal conductivity of the CRT panel glass, J. Non-Cryst. Solids 465 (2017) 59–64.
[25] J. König, R.R. Petersen, Y. Yue, D. Suvorov, Gas-releasing reactions in foam-glass formation using carbon and Mn_xO_y as the foaming agents, Ceram. Int. 43 (2017) 4638–4646.
[26] Østergaard M.B.; Cai B.; Petersen R.R.; König J.; Lee P.D.; Yue Y., Impact of pore size on thermal conductivity of glass foams. (under review)
[27] S. Köse, G. Bayer, Schaumbildung im system altglas-SiC und die eigenschaften derartiger schaumgläser, Glas. Ber. 55 (1982) 151–160.
[28] J.P. Wu, A.R. Boccaccini, P.D. Lee, R.D. Rawlings, Thermal and mechanical properties of a foamed glass-ceramic material produced from silicate wastes, Proc. Eighth Eur. Soc. Glas. Sci. Technol. Conf. Glas. Technol. Eur. J. Glas. Sci. Technol. A. 48 (2007) 133–141.
[29] D.C. Jana, G. Sundararajan, K. Chattopadhyay, Effect of porosity on structure, Young's modulus, and thermal conductivity of SiC foams by direct foaming and gelcasting, J. Am. Ceram. Soc. 100 (2017) 312–322.
[30] J. König, R.R. Petersen, Y. Yue, Fabrication of highly insulating foam glass made from CRT panel glass, Ceram. Int. 41 (2015) 9793–9800.
[31] M. Bockowski, P. Strak, I. Grzegory, S. Porowski, High pressure solution growth of gallium nitride, in: D. Ehrentraut, E. Meissner, M. Bockowski (Eds.), Technol. Gall. Nitride Cryst. Growth, Springer, Berlin Heidelberg, 2010, pp. 207–234.
[32] V. Bohac, M.K. Gustavsson, L. Kubicar, S.E. Gustafsson, Parameter estimations for measurements of thermal transport properties with the hot disk thermal constants analyzer, Rev. Sci. Instrum. 71 (2000) 2452–2455.
[33] Y. He, Rapid thermal conductivity measurement with a hot disk sensor: part 1. Theoretical considerations, Thermochim. Acta 436 (2005) 122–129, https://doi.org/10.1016/j.tca.2005.06.026.
[34] E.Y. Litovsky, M. Shapiro, Gas pressure and temperature dependences of thermal conductivity of porous ceramic materials: part 1, refractories and ceramics with porosity below 30%, J. Am. Ceram. Soc. 75 (1992) 3425–3439.
[35] E. Litovsky, M. Shapiro, A. Shavit, Gas pressure and temperature dependences of thermal conductivity of porous ceramic materials: part 2, refractories and ceramics with porosity exceeding 30%, J. Am. Ceram. Soc. 79 (1996) 1366–1376.
[36] M. Yorizane, S. Yoehlmura, H. Masuoka, H. Yoshida, Thermal conductivity of pure gases at high pressures by use of a coaxial cylindrical cell, Ind. Eng. Chem. Fundam. 22 (1983) 454–458.
[37] A. Wassiljewa, Heat conduction in gaseous mixtures, Phys. Z. 5 (1904) 737–742.
[38] A. Michels, J.V. Sengers, L.J.M. Van De Klundert, The thermal conductivity of argon at elevated densities, Physica. 29 (1963) 149–160.
[39] A. Michels, A. Botzen, The thermal conductivity of nitrogen at pressures up to 2500 atmospheres, Physica. 19 (1956) 585–598.
[40] A. Michels, J.V. Sengers, P.S. van der Gulik, The thermal conductivity of carbon dioxide in the critical region, Physica. 28 (1962) 1216–1237.
[41] E.A. Mason, S.C. Saxena, Approximate formula for the thermal conductivity of gas mixtures, Phys. Fluids 1 (1958) 361–369.
[42] J.P. Polling, B.E. Prausnitz, J.M. O'Connell, The Properties of Gases and Liquids, Fifth McGraw-Hill, New York, 2001.
[43] M. Yorizane, S. Yoshimura, H. Masuoka, H. Yoshida, Thermal conductivities of binary gas mixtures at high pressures: nitrogen-oxygen, nitrogen-argon, carbon dioxide-argon, and carbon dioxide-methane, Ind. Eng. Chem. Fundam. 22 (1983) 458–463.
[44] M.B. Østergaard, R.E. Youngman, M.N. Svenson, S.J. Rzoska, M. Bockowski, L.R. Jensen, M.M. Smedskjaer, Temperature-dependent densification of sodium borosilicate glass, RSC Adv. 5 (2015) 78845–78851.